

UCLA

UCLA Previously Published Works

Title

Stabilizing *CO₂ Intermediates at the Acidic Interface using Molecularly Dispersed Cobalt Phthalocyanine as Catalysts for CO₂ Reduction

Permalink

<https://escholarship.org/uc/item/11x151wt>

Journal

Angewandte Chemie International Edition, 63(8)

ISSN

1433-7851

Authors

Feng, Shijia

Wang, Xiaojun

Cheng, Dongfang

et al.

Publication Date

2024-02-19

DOI

10.1002/anie.202317942

Copyright Information

This work is made available under the terms of a Creative Commons Attribution-NonCommercial-NoDerivatives License, available at

<https://creativecommons.org/licenses/by-nc-nd/4.0/>

Peer reviewed

Stabilizing *CO₂ Intermediates at the Acidic Interface using Molecularly Dispersed Cobalt Phthalocyanine as Catalysts for CO₂ Reduction

Shijia Feng^{1,7}, Xiaojun Wang^{1,2,7}, Dongfang Cheng^{4,7}, Yao Luo^{3,7}, Mengxin Shen¹, Jingyang Wang¹, Wei Zhao¹, Susu Fang³, Hongzhi Zheng¹, Liyao Ji¹, Xing Zhang¹, Weigao Xu³, Yongye Liang⁶, Philippe Sautet^{4,5}, Jia Zhu^{1,2*}

¹National Laboratory of Solid State Microstructures, Collaborative Innovation Center of Advanced Microstructures, College of Engineering and Applied Sciences, Nanjing University, Nanjing, Jiangsu 210023, P. R. China.

²School of Sustainable Energy and Resources, Nanjing University, Suzhou 215163, P.R. China

³Key Laboratory of Mesoscopic Chemistry of Ministry of Education, School of Chemistry and Chemical Engineering, Nanjing University, Nanjing, 210023 P. R. China

⁴Department of Chemical and Biomolecular Engineering, University of California, Los Angeles, Los Angeles, California 90095, United States

⁵Department of Chemistry and Biochemistry, University of California, Los Angeles, Los Angeles, California 90095, United States

⁶Department of Materials Science and Engineering, Guangdong Provincial Key Laboratory of Energy Materials for Electric Power, Southern University of Science and Technology, Shenzhen, China

⁷These authors contributed equally to this work.

*Correspondence: jiazhu@nju.edu.cn

Abstract: CO₂ electroreduction (CO₂R) operating in acidic media circumvents the problems of carbonate formation and CO₂ crossover in neutral/alkaline electrolyzers. Alkali cations have been universally recognized as indispensable components for acidic CO₂R, while they cause the inevitable issue of salt precipitation. It is therefore desirable to realize alkali-cation-free CO₂R in pure acid. However, without alkali cations, stabilizing *CO₂ intermediates by catalyst itself at the acidic interface poses as a challenge. Herein, we first demonstrate that a carbon nanotube-supported molecularly dispersed cobalt phthalocyanine (CoPc@CNT) catalyst provides the Co single-atom active site with energetically localized *d* states to strengthen the adsorbate-surface interactions, which stabilizes *CO₂ intermediates at the acidic interface (pH = 1). As a result, we realize CO₂ conversion to CO in pure acid with a faradaic efficiency of 60% at pH = 2 in flow cell. Furthermore, CO₂ is successfully converted in cation exchanged membrane-based electrode assembly with a faradaic efficiency of 73%. For CoPc@CNT, acidic conditions also promote the intrinsic activity of CO₂R compared to alkaline conditions, since the potential-limiting step, *CO₂ to

*COOH, is pH-dependent. This work provides a new understanding for the stabilization of reaction intermediates and facilitates the designs of catalysts and devices for acidic CO₂R.

Introduction

Renewable electricity-powered CO₂ reduction (CO₂R) offers a low-carbon-footprint route to realize the conversion from CO₂ to valuable chemicals and fuels.^[1] The neutral and alkaline electrolyzers provide locally alkaline conditions to realize CO₂R with high selectivity versus hydrogen evolution reaction (HER).^[2] However, under the combined effects of non-faraday reaction and electric field,^[3] carbonate formation and CO₂ crossover lead to a mixture of O₂ and CO₂ at the anode,^[4] therefore subsequent energy-intensive and costly gas separation and CO₂ recovery processes are required.

The acidic flow cell, where the catalyst is in contact with the acidic media, provides a promising route to suppress the carbonate formation and thus circumvent CO₂ crossover.^[5] However, CO₂ reduction cannot take place in pure acid where hydrogen evolution reaction (HER) dominates, since *CO₂ intermediates are difficult-to-stabilize under the condition of high proton concentration.^[4, 6] This problem can be overcome by the addition of alkali cations,^[7] which construct a locally alkaline environment at the catalyst surface to suppress HER activities^[4, 8] and lower the CO₂ adsorption energy so as to stabilize *CO₂ intermediates.^[6c] To match the acidic environment^[9] and eliminate the resistance of catholyte^[10] in acidic flow cells for large scale application, cation exchange membrane (CEM) can be employed in membrane electrode assemblies, denoted as CMEA.^[2a, 9, 11] Although alkali cations can suppress HER and promote CO₂R in acidic flow cells, it has recently been proven that the salt precipitation induced by alkali cations is inevitable during the electrolysis process.^[12] This problem becomes even more severe in CMEA without liquid flow at the cathode, which leads to premature device death.^[2a] Up to now, no CO₂R activity and 100% H₂ selectivity has been observed in CMEA without alkali cations, which is also attributed to the unstable *CO₂ intermediates at the acidic surface. To realize a high-performance CO₂R in CMEA, stabilizing *CO₂ intermediates in pure acid without alkali cations is necessary. Very recently, concurrent researches reported the immobilized organic cations replacing alkali cations to enable metal-free CO₂ reduction in pure acid.^[13] It should be noted that immobilized organic cations are drawn by the long chains, making it difficult to ensure that all catalytic sites can be adequately covered by immobilized organic cations. HER will dominate on uncovered catalysts owing to the unstable *CO₂ intermediates. Moreover, as the current density increases, the surface alkalinity constructed by immobilized organic cations gradually decreases, leading to an obvious decline in CO₂ selectivity. To reduce the dependence of CO₂R on additional cations, including metal and organic cations, stabilizing *CO₂ intermediates by catalyst itself at the acidic interface is crucial but still currently lacking.

Herein, we report CO₂ conversion towards CO in pure acid using a carbon nanotube-supported molecularly dispersed cobalt phthalocyanine (CoPc@CNT). The Co single-atom active sites with energetically localized *d* states strengthens the adsorbate-surface interactions, which effectively stabilizes the *CO₂ intermediates at the acidic interface. The key for a good CO₂ conversion is to render the chemisorbed *CO₂ intermediate as stable, or even better more stable than H.^[14] Density functional theory (DFT) calculations reveal that CO₂ adsorption competes with H adsorption on CoPc@CNT even at pH = 1, while the CO₂ adsorption step is completely suppressed by the high coverage of H on Au and Ag (Figure 1). As a result, CoPc@CNT experimentally exhibits a faradaic efficiency (FE) of 60% for CO in acidic flow cell (pH = 2) and enables CO₂ conversion in CMEA with a CO-FE of as high as 73%, while classic catalysts Au and Ag show no CO₂R activity. In addition, the proton coupled electron transfer step, i.e., *CO₂ to *COOH, which is consistently confirmed by electrochemistry analysis with *in situ* Raman spectroscopy, is also proved to be the potential-limiting step on CoPc@CNT, rationalizing the lower overpotential (320 mV at 30 mA/cm²) in the acidic compared to alkaline conditions.

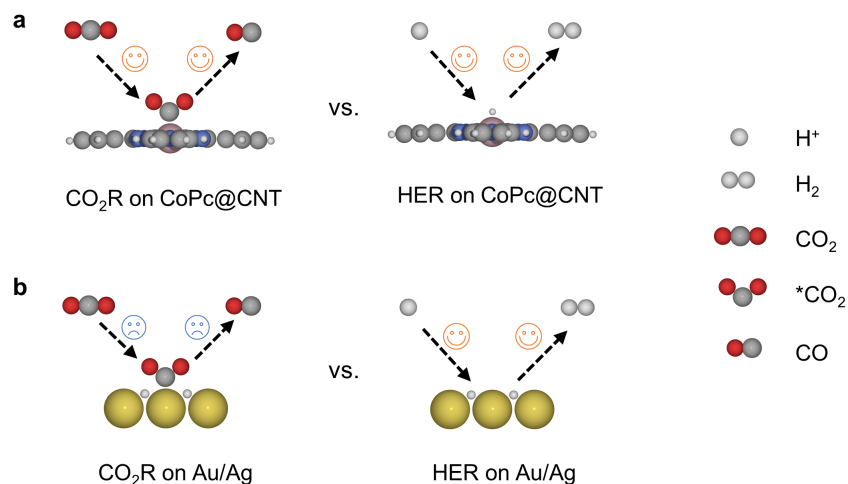


Figure 1. CO₂ adsorption competing with H adsorption on catalyst at the acidic interface. (a-b) Schematic of CO₂R and HER on (a) CoPc@CNT and (b) Au/Ag in pure acid without alkali cations. The *CO₂ intermediate can be stabilized at the surface of CoPc@CNT for further reduction since CO₂ adsorption can compete with H adsorption. As for Au and Ag, H adsorption is more facile than CO₂ adsorption, resulting in a destabilized *CO₂ adsorption and boosted HER.

Results and Discussion

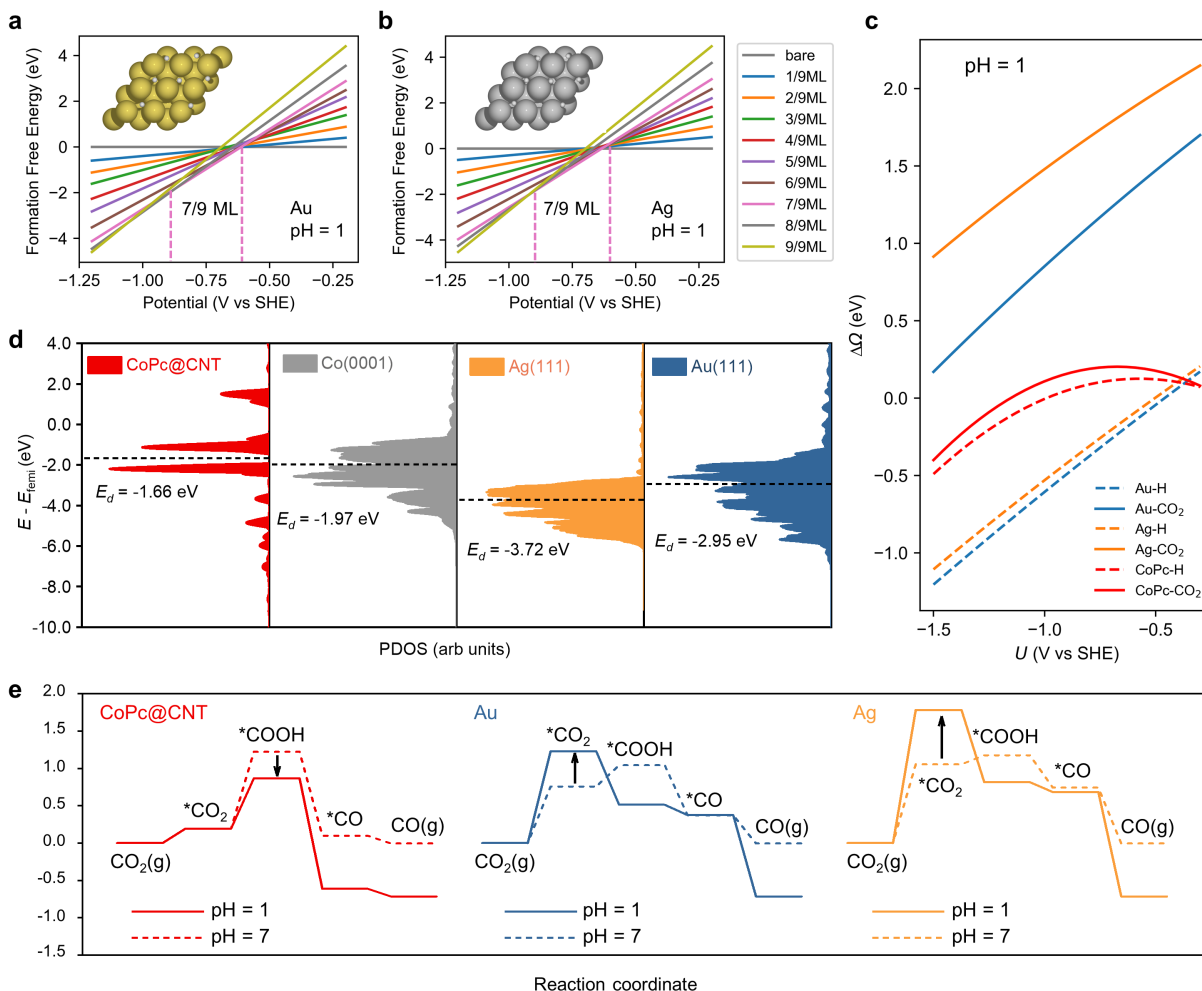


Figure 2. Theoretical insights for CO₂ reduction at the acidic interface. (a-b) Formation free energy for H adsorption on (a) Au and (b) Ag as the function of potential at pH = 1. (c) Adsorption free energy of *H and *CO₂ on Au, Ag and CoPc@CNT as the function of potential at pH = 1. In the case of Au and Ag, the surfaces are therefore H-covered at the relevant potential for CO₂ reduction. Regarding the CoPc@CNT, the Co atom active site will either adsorb *H or *CO₂ in roughly similar proportion, since adsorption free energies are similar. (d) Projected density of states of *d* states of CoPc@CNT, Co(0001), Ag(111) and Au(111). Compared with metal catalysts, CoPc@CNT shows a narrower *d* state and a higher *d*-band center (E_d). (e) The free energy diagram of CO₂R pathway on CoPc@CNT and Au/Ag at -0.7 V vs. SHE at pH = 1 and 7.

Single-atom catalysts generally show stronger adsorption towards CO₂R reaction intermediates compared to bulk catalysts.^[15] Unlike other single-atom catalysts with complicated synthesis steps at high temperature, CoPc@CNT is easy to be prepared at mild condition and thus have a clear metal-N₄

coordination structure, providing an excellent model catalyst for theoretical calculations.^[16] Among the metal phthalocyanines, CoPc can realize high-performance CO₂R in neutral and alkaline conditions without a further structure regulation.^[2c, 10, 17] It is anticipated that CoPc@CNT, featuring Co single-atom active sites, has the potential to enhance stabilization of CO₂ intermediates, enabling CO₂ conversion in pure acid without alkali cations. Meanwhile, Au and Ag which are known as the classic bulk metal catalysts for CO₂ conversion to CO in neutral and alkaline conditions, are selected as the comparison samples.^[18] To predict the CO₂R activity and reaction pathway of single-atom catalyst CoPc@CNT and bulk catalysts (Au and Ag) in pure acid, DFT calculations are first employed in this study.

For bulk catalysts Au and Ag, it is imperative to consider the H coverage prior to assessing the adsorption of reaction intermediates. In pure acid, since the pH are quite low, the protons are much more active than in alkaline solution, which indicates that the catalyst surface will undergo quick exchange of H with solution, leading to boosted hydrogen evolution reaction (HER). The fast dynamics is usually associated with high H coverage at equilibrium. Nonetheless, previous theoretical studies mainly focus on CO₂R catalytic process on the bare Au or Ag surface without H co-adsorption.^[6c, 15a] Our calculations, however, reveal that under acidic conditions, the catalyst surfaces are predominantly covered with H, which may strongly affect the energetics of CO₂R pathway. In the case of Au(111), the H coverage will quickly reach up to 7/9 monolayer (ML) at -0.61 V vs. SHE, before which the surface maintains its pristine clean state (**Figure 2a**). As the potential becomes more negative than -0.88 V vs. SHE, the H coverage will increase consequently and reach 1 ML. A similar phenomenon can be seen on Ag(111) surface (**Figure 2b**). As illustrated in **Figure 2a and 2b**, the Au and Ag surfaces are decorated with a high coverage of H in acidic conditions, whereas they tend to be clean at moderate potentials in alkaline media (**Figure S1 and S2**).

The competitive adsorption of H and CO₂ is crucial for the selectivity between HER and CO₂R. We then evaluate the adsorption energy of H and CO₂ at pH = 1 on H-covered Au, Ag and CoPc@CNT catalysts using grand canonical DFT, which allows explicit surface charging with an implicit electrolyte model. As illustrated in **Figure 2c**, for Au and Ag, the surfaces being covered with H make CO₂ adsorption extremely difficult, featured by high reaction energies of 1.20 eV and 1.75 eV at -0.7 V vs SHE, respectively. If CO₂ is unable to adsorb onto the catalyst surface, the following CO₂R reaction cannot take place, whereas HER will be dominating at the given condition. For CoPc@CNT, the Co atom active site can either adsorb *CO₂ or *H with roughly similar probabilities. The single Co site cannot stabilize 2*H during optimization, and such structure quickly undergoes the Tafel step to form H₂. Thus, for CoPc/CNT, a fraction of the Co active sites can interact with CO₂ at the potential for CO₂ reduction. Based on this, on CoPc@CNT (model in **Figure S3**), even at pH = 1, CO₂ adsorption can compete with H adsorption and exhibit a similar adsorption energy across a large potential range, indicating that CoPc@CNT is still active toward CO₂ reduction, rather than being occupied by *H in acidic solution. The strong CO₂ adsorption on CoPc@CNT can be attributed

to the unique electronic structure of the Co single-atom site, which shows the much more energy localized $3d$ state compared to the dispersed d band states for bulk Co (Figure 2d). According to the Newns–Anderson–Grimley model, the hybridization between the adsorbates and the s state of metal leads to a broadened adsorbate state, while such state will split into localized bonding and antibonding states when hybridizing with d state of metal. A energy localized d state will result in a stronger interaction between the adsorbate and the metal.^[15a, 19] In addition, since the energy separation between the metal d states and the H $1s$ orbital is larger than that with the C $2p$ orbital, the perturbative strength is correspondingly smaller for the H $1s$ bonding orbital.^[20] This means that more energy localized d states will have a more significant effect on *CO_2 bonding compared with H bonding.

The pH effects on reaction pathway are explored by comparing the energy profile of CO_2R at pH = 1 with pH = 7 (Figure 2e). For Au and Ag, at pH = 1, although the steps after CO_2 adsorption are all exothermic, the high barrier of CO_2 adsorption limits the CO_2R activity. In neutral condition (pH = 7), Au and Ag surfaces will not be covered with *H , and it can be found that CO_2 adsorption will be much easier than that in acidic condition. As for CoPc@CNT, the energy of *CO_2 protonation step (from *CO_2 to *COOH) is obviously higher than that of CO_2 adsorption step (from CO_2 to *CO_2), indicating that the potential-limiting step is the protonation of *CO_2 to *COOH . Previous work showed that the relative energy of CO_2 adsorption and *CO_2 protonation step is decisive factor in determining the pH-dependent behavior.^[15a] Specifically, if $\Delta G(CO_2 \text{ to } ^*CO_2) > \Delta G(^*CO_2 \text{ to } ^*COOH)$, a pH-independent behavior is observed because CO_2 adsorption will be the potential-limiting step, whereas a converse scenario is encountered when $\Delta G(CO_2 \text{ to } ^*CO_2) < \Delta G(^*CO_2 \text{ to } ^*COOH)$, since *COOH formation involves coupled proton and electron transfer. Accordingly, DFT calculations reveal that CO_2R is pH-dependent for CoPc@CNT, which is consistent with previous reports.^[15a, 16, 21] As a result, the reaction energy in an acidic condition (0.68 eV, pH = 1) is lower than that in a neutral condition (1.03 eV, pH = 7). Based on the above results, DFT calculations suggest that Au and Ag exhibit remarkable CO_2R activity in alkaline condition but cannot compete with HER in acidic solution due to the difficult CO_2 adsorption on H-covered surfaces. In contrast, on CoPc@CNT, the *CO_2 intermediate can be stabilized in acidic conditions and lowering the pH will favor the potential-limiting step and decrease the overpotential of CO_2R .

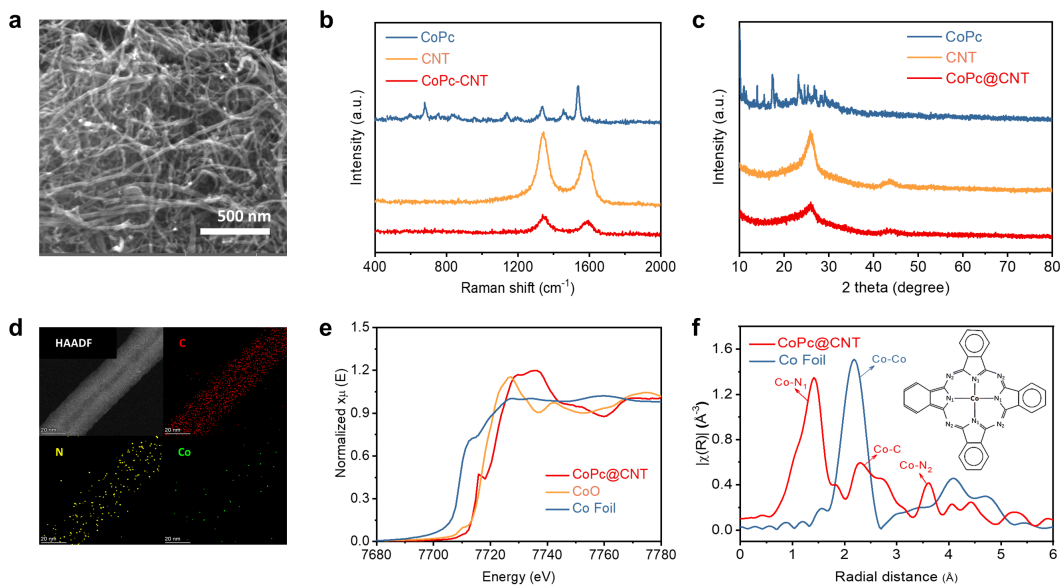


Figure 3. Synthesis and Characterizations of single-atom catalyst CoPc@CNT. (a) SEM images of CoPc@CNT. (b) XRD patterns and (c) Raman spectra of CoPc particle, CNT and CoPc@CNT. (d) EDS elemental maps of CoPc@CNT. (e) Co K-edge XANES spectra of CoPc@CNT, Co Foil and CoO. (f) Co K-edge EXAFS spectra of CoPc@CNT and Co Foil.

To verify the above theoretical predictions, the single-atom catalyst CoPc@CNT is fabricated by mixing the multi-walled carbon nanotubes (CNT) and CoPc-saturated DMF solution with magnetic stirring, during which CoPc molecules can be anchored on CNT via strong π - π interactions. It should be noted that CoPc-saturated solution instead of CoPc-supersaturated solution is used in this work, ensuring that all CoPc molecules are dispersed over CNT at the molecular level rather than forming self-accumulating clusters, which is also aligned with the computational single-atom structure model. This point is confirmed by scanning electron microscopy (SEM) images, in which only CNT is observed when using CoPc-saturated solution (**Figure 3a**), while obvious CoPc particles are present when CoPc-supersaturated solution is used according to previous work^[22] (**Figure S4**). From X-ray diffraction (XRD) patterns (**Figure 3b**), CoPc@CNT shows only CNT diffraction peaks without the signals of CoPc, inferring that CoPc molecules are dispersed on CNT without forming CoPc crystals. Similar result is also demonstrated from the Raman spectra (**Figure 3c**), where only D band and G band of CNTs are probed at 1350 and 1590 cm^{-1} . Moreover, the Energy-dispersive X-ray spectroscopy (EDS) elemental maps (**Figure 3d**) also demonstrate a high-level distribution of Co over the CNTs substrates. To identify the local electronic structure and chemical environment of Co metal in CoPc@CNT, X-ray absorption near-edge structure (XANES) (**Figure 3e**) and Fourier-transformed extended X-ray adsorption fine structure (EXAFS) (**Figure 3f**) analyses are performed.

As shown in **Figure 3e**, the adsorption edge position of CoPc@CNT is close to that of CoO, suggesting that the oxidation state of Co atom in CoPc@CNT is similar to that in CoO (+2). In EXAFS curves (**Figure 3f**), the peak of around 1.41, 2.30 and 3.61 Å in CoPc@CNT are assigned to Co-N₁, Co-C and Co-N₂ signals,^[23] while no Co-Co bonding signal is observed indicating that the as-prepared CoPc@CNT in this work is indeed a single-atom catalyst. To avoid CO₂ mass transfer limitations,^[24] the CoPc@CNT gas diffusion electrode is fabricated by loading CoPc@CNT onto hydrophobic carbon paper with Nafion binder. In addition, bulk metal catalysts Au and Ag catalysts are fabricated by magnetron sputtering.

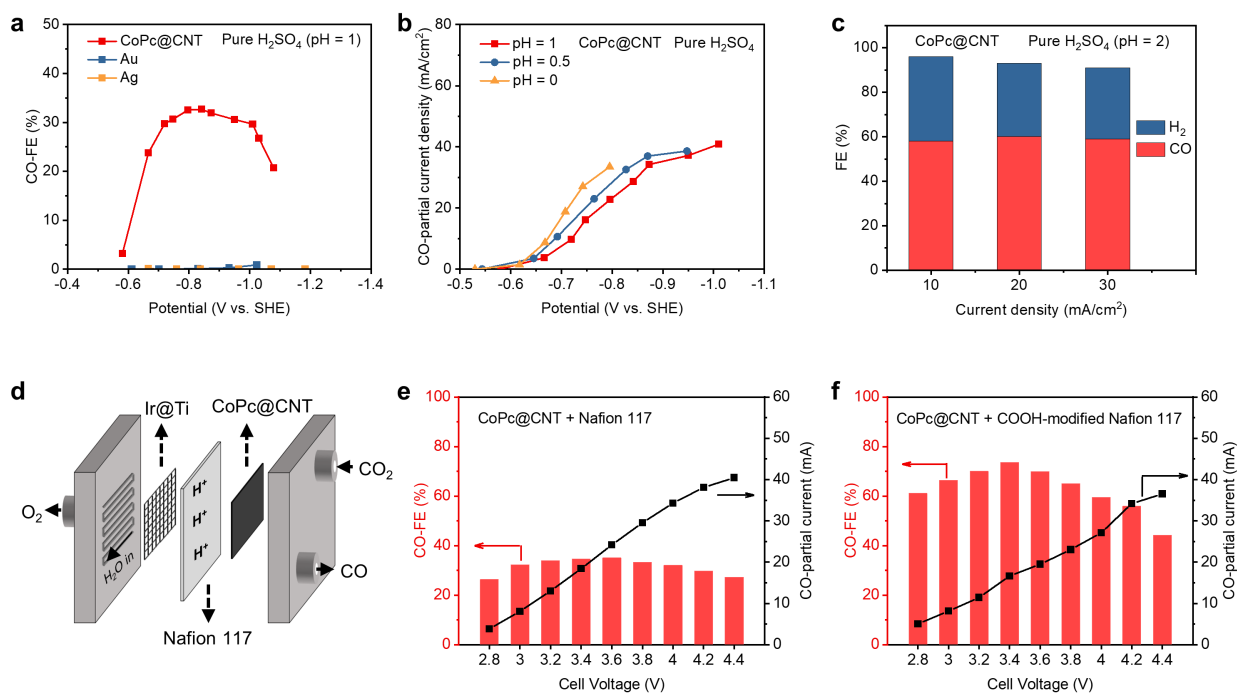


Figure 4. Catalytic activity of CoPc@CNT at the acidic interface. (a) CO-FE comparison of CoPc@CNT, Au and Ag in pure H₂SO₄ electrolyte (pH = 1) under different applied potentials using flow cell. (b) CO-partial current densities of CoPc@CNT in pure acid (pure H₂SO₄ electrolyte, pH = 0, 0.5 and 1) under different applied potential using flow cell. (c) FE of CO and H₂ on CoPc@CNT in pure H₂SO₄ electrolyte (pH = 2) under different current densities using flow cell. (d) Schematic of CMEA device for CO₂ reduction. (e) CO-FE and CO-partial current of CoPc@CNT under different cell voltages using CMEA. (f) CO-FE and CO-partial current of CoPc@CNT at varied cell voltages in CMEA when Nafion membrane is modified by carboxyl groups (-COOH).

To confirm the successful fabrication of gas diffusion electrodes (GDE), CO₂R experiments are performed in neutral catholyte (CO₂-saturated 1 M KHCO₃, pH = 7.8), and the faradic efficiency of CO

(denoted as CO-FE) as a function of potential is shown in **Figure S5-S7**. The Au electrode shows a CO-FE of around 70% from -1.0 to -1.8 V vs. SHE, and the Ag electrode exhibits a CO-FE of 90% at -1.73 V vs. SHE, which is consistent with literature.^[25] Meanwhile, the CoPc@CNT electrode presents a CO-FE of nearly 100% from -1.0 V to -1.4 V vs. SHE. The above results indicate that the obtained electrodes enable highly efficient conversion from CO₂ to CO in neutral media, and also confirm the effectiveness of the gas diffusion electrode in flow cell.

The evaluation of CO₂R performance in pure acid is carried out respectively on Au, Ag and CoPc@CNT electrodes. In flow cells, both catholyte and anolyte are sulfuric acid aqueous solution (pH = 1), furthermore, the electrolyte differs from previous works in that no alkali cations are added.^[4, 7a, 8, 18b] Although alkali cations can suppress HER and enhance CO₂R in flow cell, it is not suitable for CMEA due to the salt precipitation.^[2a] Nafion 117 is employed to separate catholyte and anolyte, as well as for facilitating the transport of protons. Ir@Ti mesh is used as the counter electrode to realize the water oxidation reaction in acidic media. Since the catalyst can maintain stability during short-term testing, a complete polarization curve can be obtained by a single catalyst (**Figure S8**). As shown in **Figure 4a** and **S9**, a CO-FE of ~32% is obtained at -0.8 V vs. SHE for CoPc@CNT. However, no CO₂ activities are observed on both Au and Ag electrodes (**Figure S10-S11**). These results are consistent with the above theoretical predictions that CoPc@CNT instead of Au and Ag can drive CO₂ conversion in pure acid due to the strong CO₂ adsorption (**Figure 2**). In addition, both excessive (FePc@CNT) and insufficient (NiPc@CNT and Ni@N-doped carbon) interactions with the reaction intermediate are unfavorable for pure acidic CO₂R (**Figure S12**), and further explorations are needed to understand the selectivity differences among single-atom catalysts. Regardless, the stability of *CO₂ intermediate is necessary for acidic CO₂R in the absence of alkali cations.

The CO₂R activities of CoPc@CNT are further explored in different acidic conditions. Even under more acidic conditions (pH = 0.5 and 0), CoPc@CNT stabilizes the reaction intermediates to enable CO₂ conversion (**Figure 4b**). The reaction potential of CO₂R shifts positively with a decrease in acidity, aligning with our theoretical calculations, indicating that CO₂R is pH-dependent for CoPc@CNT. However, HER is enhanced dramatically as the acidity increase, resulting in obvious decreases of CO-FE (**Figure S13**). On the contrary, HER is effectively suppressed by reducing the proton concentration thus a notable CO-FE of 60% is achieved at pH = 2 (**Figure 4c** and **S14**). Due to the low ionic conductivity and the large ohm resistance, CO₂R is difficult to be operated under a higher current density and a weaker acidic condition (**Figure S15**) in flow cells.

CMEA is an easily scale-up device which can efficiently minimize the ohmic loss of electrolyte in flow cells (**Figure S16**).^[2a, 11] For CMEA device (**Figure 4d**), cation exchange membrane is placed between cathode and anode as solid electrolyte, through which the protons generated at the anode transport to the

cathode to participate in CO₂R. In addition, ultra-pure water as the anolyte flows into the anode chamber, which can avoid the interference of impurity cations on cathodic CO₂R reaction. As shown in **Figure 4e**, a CO-FE of around 36% is obtained at 2.8 V, which is similar to that of CO₂R performed in flow cells at pH = 1 (**Figure 4c**). The stability test of MEA is performed at 3.4 V, and it still maintains 80% of the initial CO-FE after 13-hour operation (**Figure S17**). The decrease in CO₂ selectivity is primarily attributed to catalyst deactivation, and this issue is expected to be improved through substituent group modifications according to the previous report.^[26] To improve the CO₂ selectivity by weakening the surface acidity of Nafion membrane, polyethylene microporous separator (thickness of 32 μm) with traces of acetic acid (CH₃COOH) aqueous solution (pH = 3) is introduced between CoPc@CNT and Nafion membrane. The CO-FE has shown a significant improvement, increasing from 36% to 52%, as depicted in **Figure S18**. To overcome the issue of acetic acid volatilization while retaining its function in reducing the surface acidity of the Nafion membrane, carboxyl groups (-COOH) are modified onto the surface of the Nafion membrane through a combination of electrostatic assembly and chemical reactions, as illustrated in **Figure S19**. The increased electrochemical impedance suggests that the COOH groups have been successfully modified onto the surface of the Nafion membrane (**Figure S20**), achieving the desired effect of reducing surface acidity. After the modification, the CO-FE exceeds 60% across a wide voltage range (2.8-4.0 V), with the highest value reaching up to 73% at 3.4 V (**Figure 4f and S21**). Comparing the changes in partial currents and FE of H₂ and CO before and after COOH modification (**Figure S22**), the increase in CO-FE is due to the COOH group inhibiting HER rather than enhancing CO₂R. Meanwhile, the protonation process is the potential-limiting step for CO₂R on CoPc@CNT, leading to a decrease in CO partial current density after COOH modification. From the above, we successfully realize CO₂ conversion in CMEA using CoPc@CNT.

Obviously, there are still some unresolved issues, particularly concerning the issue of CO-partial current density. This issue presents two main challenges. Firstly, at high applied potentials, the higher proton concentration at the catalyst surface enhances the adsorption of H, thereby inhibiting CO₂ adsorption and leading to decreased CO₂R selectivity. Secondly, the multi-step nature of the CO₂R process may be slower than the competing HER, even under similar adsorption energy, favoring HER selectivity. We believe that addressing this issue solely from the catalyst's perspective is challenging at present, but there is hope for resolving it by combining control of the surface microenvironment. In this work, the introduction of organic cations onto the catalyst's surface is proven to be an effective strategy for enhancing the CO-partial current density (**Figure S23**). Relative to the non-additive condition, the addition of 0.2 M tetramethylammonium chloride significantly increases the CO-partial current density from 34 mA/cm² to 71 mA/cm² in flow cell. Under high current conditions, the organic cations of tetramethylammonium will encounter the same issue as alkali metal ions, which is the formation of bicarbonate precipitates, resulting in a decrease in CO

selectivity. This issue can be overcome by cross-linking for organic cations, which has already been verified by concurrent research.^[13b] It should be noted that the immobilized organic cations are drawn by the long chains, making it difficult to ensure that all catalytic sites can be adequately covered by immobilized cations. HER will dominate on uncovered catalysts owing to the unstable CO₂ intermediates. Thus, it is expected that the catalyst itself can stabilize CO₂ intermediates and reduce its dependence on the surface microenvironment, which is exactly what the article aims to emphasize. From the above, to achieve a more significant improvement in selectivity and current density for metal-free acidic CO₂ reduction, it is necessary to integrate catalyst design with microenvironment control.

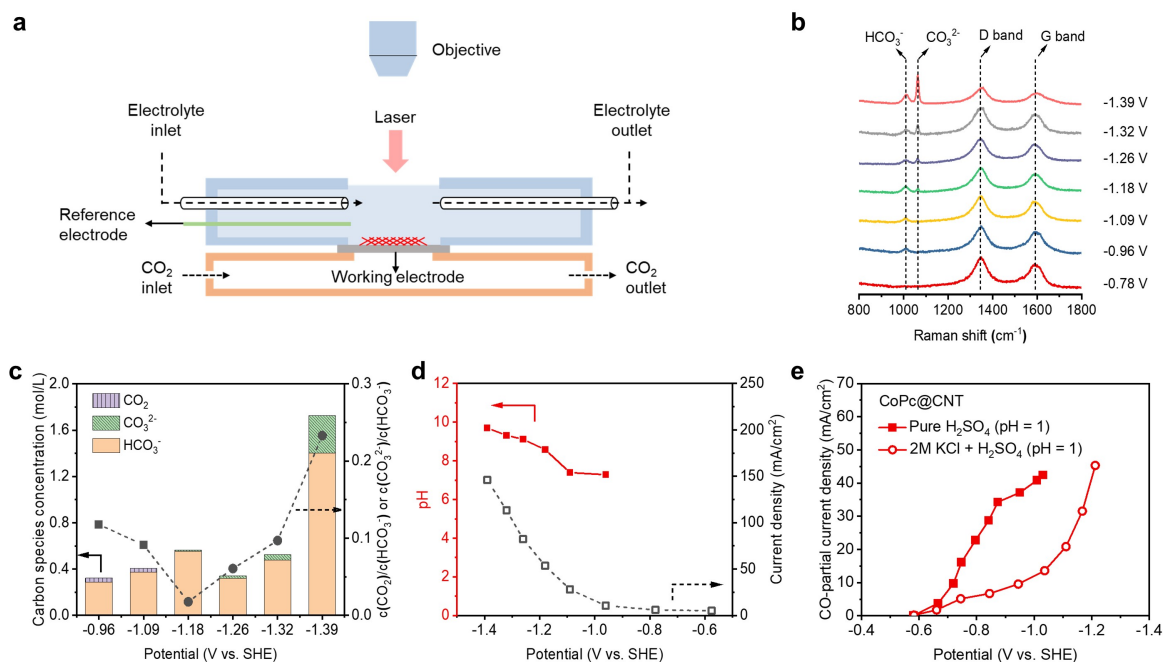


Figure 5. Experimental verification of the potential-limiting step. (a) Schematic diagram of *in situ* electrochemical Raman test. (b) Raman spectra of CoPc@CNT in 2.0 M KCl aqueous solution (pH = 1) under different applied potentials. (c) Carbon species concentrations derived from the spectra in b and the ratio of CO₂/HCO₃⁻ (square) and CO₃²⁻/HCO₃⁻ (circle) under different applied potentials. (d) pH profile derived from carbon species ratio in c and current density under different applied potentials. (e) CO-partial current densities of CoPc@CNT in acidic catholyte (pH = 1) with or without highly concentrated K cations under the different density using flow cell.

DFT calculations reveal that the protonation of *CO₂ to *COOH step is the potential-limiting step for CoPc@CNT (Figure 2e), meaning that reducing the proton concentration (i.e., increasing the local pH) at the catalyst surface will increase the reaction barrier. Although pH dependence of the electrochemical

reaction can be explored by changing the bulk pH,^[15a] this method neglects the variation in local pH under the electrolysis, so the conclusions obtained may not be accurate. To avoid this problem, we combine electrochemistry analysis with *in situ* Raman spectroscopy to investigate the relationship between overpotential and local pH. If the protonation process is the potential-limiting step, a higher overpotential is expected when local pH increases. Herein, the overpotential can be obtained by electrochemistry analysis, and local alkalinity is constructed by adding highly concentrated K⁺,^[4, 27] which can be quantitatively probed by *in situ* Raman spectroscopy.

The schematic representation of *in situ* electrochemical Raman spectroscopy is depicted in **Figure 5a** and **S24**. In this study, HCO₃⁻ and CO₃²⁻ are selected as pH probes because they are the products of the CO₂-OH⁻ neutralization reaction,^[28] which avoids any interference from incorporating additional pH-sensitive species. **Figure 5b** shows the Raman spectra with different cathodic potential (from -0.78 to -1.39 V vs. SHE) in K-containing acidic media (2.0 M KCl in HCl aqueous solution, pH = 1). The pronounced peaks of around 1350 and 1590 cm⁻¹ are attributed to D band and G band of the carbon nanotube, which indicates successful focusing of the light spot on the catalyst. In the spectra, the Raman signals at the wavenumbers of 1012 and 1064 cm⁻¹ are assigned to HCO₃⁻ and CO₃²⁻ vibrational modes, respectively. Since the reaction is conducted under the condition of pH = 1, HCO₃⁻ and CO₃²⁻ are not present in the initial reaction solution even when a low potential is applied (-0.78 V). They are only produced in the regions of catalyst surface and diffusion layer when the potential reaches -0.96 V or higher. Although surface enhancement effects were not employed, combining the testing principle with the actual conditions reveals that the Raman signals of HCO₃⁻ and CO₃²⁻ originate from the region near the catalyst. The distinct Raman features of HCO₃⁻ and CO₃²⁻ ensure that they can be independently quantified using calibration curves (**Figure S25**), and their corresponding concentration as a function of potential are illustrated in **Figure 5c**. The CO₂ concentration is originated from the reasonable assumption, according to previous report^[29]. CO₂ and CO₃²⁻ cannot coexist in water, and pH = 8.37 is a threshold value, as shown in **Figure S26**. When the CO₃²⁻ signal is not observed in Raman spectra, and considering the continuous supply of gaseous CO₂ (1 bar), the dissolved CO₂ is assumed to be a constant saturation concentration of 0.033 M. Conversely, when the CO₃²⁻ signal is observed in Raman spectra, the concentration of dissolved CO₂ is regarded as constant at 0 M. Based on the acid-base equilibrium reactions, local pH can be further derived (**Figure 5d**). It is worth noting that the local pH is up to ~7.3 when the cathodic potential is -0.96 V vs. SHE with the low current density of 10.53 mA/cm². This high pH value can be attributed to K⁺ cations, which modulate the distribution of electric field in the double layer and thus suppress the migration of hydronium ions.^[4] Moreover, a higher local pH is also observed at a more negative potential. The calculated pH values based on Raman tests and assumption align perfectly with the theoretical range (**Table S1**), further validating the rationality of the assumed CO₂ values. Meanwhile, no signals of HCO₃⁻ or CO₃²⁻ are observed in alkali-

cation-free acidic CO₂R process (**Figure S27**). From above, *in situ* electrochemical Raman spectroscopy proves that highly concentrated K⁺ can induce an obvious increase of local pH. Similar trends are also observed in COMSOL simulations (**Figure S28 and S29**).

As shown in **Figure 5e** (details in **Figure S30**), overpotential shows a dramatic increase after adding highly concentration of K⁺. At the same CO-partial current density of 30 mA/cm², the applied potential of the K-containing system with high local pH (-1.16 V vs. SHE) is 320 mV higher than that of the pure acidic system with low local pH (-0.84 V vs. SHE). Combined with results from *in situ* Raman spectroscopy, a higher overpotential is observed experimentally as the local pH increases, proving that the protonation of *CO₂ to *COOH step is the potential-limiting step for CoPc@CNT (**Figure 2e**). This result is also confirmed by potential analysis with a wide pH range^[15a] and kinetic isotope experiments^[30] (**Figure S31 and S32**).

Conclusion

In summary, we demonstrate CO₂ conversion in pure acid without alkali cations using the single-atom catalyst CoPc@CNT. In this work, CoPc@CNT provides the Co single-atom active sites with energetically localized *d* states to stabilize the chemisorbed *CO₂ intermediates at the acidic interface, exhibits a faradaic efficiency of 60% in flow cells and realizes CO₂ conversion in CMEA with a CO-FE of 73%. In addition, the pH-dependent protonation of *CO₂ to *COOH is confirmed as the potential-limiting step for CoPc@CNT, thus lowering the pH will make the reaction energy of such step more favorable and drive CO₂R with a lower overpotential compared to alkaline conditions. This work not only provides a new understanding for the stabilization of *CO₂ intermediates in acidic media, but also facilitates the design of catalysts and devices for CO₂R in CMEA.

Acknowledgments

This work is jointly supported by the National Natural Science Foundation of China (Nos. 92262305, 52302225, 52202251, 51925204, 52322211), the National Key Research and Development Program of China (No. 2021YFA140070, 2022YFA1404704), Carbon Peaking and Carbon Neutrality Science and Technology Innovation Fund of Jiangsu Province (BK20220035). The authors acknowledge the micro-fabrication center of the National Laboratory of Solid State Microstructures (NLSSM) for technique support. Prof. Jia Zhu acknowledges the support from the XPLOER PRIZE. D.C. and P.S. acknowledged the National Science Foundation CBET Grant 2103116, the Audi CO₂ Cy Pres Award, and Computational resources from the Hoffman2 cluster at UCLA Institute for Digital Research and Education (IDRE). The authors sincerely thank Hua Zhou (Advanced Photon Source, Argonne National Laboratory) for his kind help in measuring X-ray absorption spectroscopy. This research used resources of the Advanced Photon

Source (12-BM), a U.S. Department of Energy (DOE) Office of Science User Facility operated for the DOE Office of Science by Argonne National Laboratory under Contract no. DE-AC02-06CH11357.

Conflict of Interest

The authors declare no conflict of interest.

Data availability

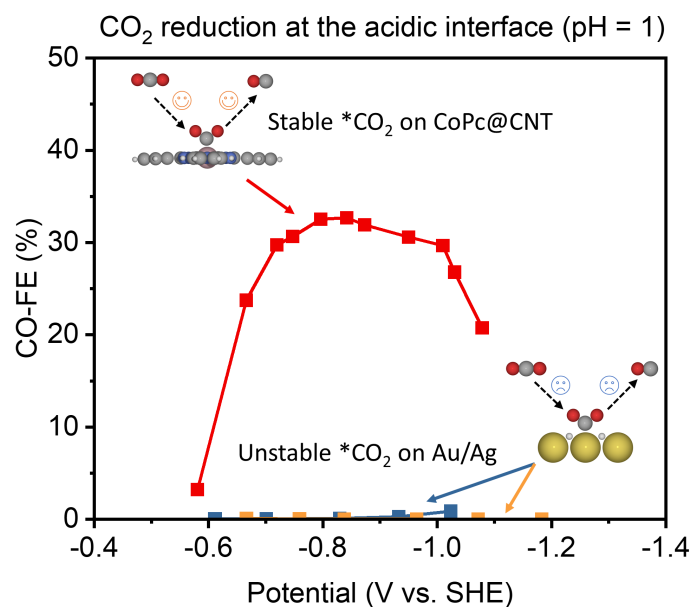
The data that support the findings of this study are available from the corresponding author upon reasonable request.

References

- [1] a) P. De Luna, C. Hahn, D. Higgins, S. A. Jaffer, T. F. Jaramillo, E. H. Sargent, *Science* **2019**, *364*, eaav3506; b) G. Zhang, L. Li, Z.-J. Zhao, T. Wang, J. Gong, *Acc. Mater. Res.* **2023**, *4*, 212-222; c) S. Nitopi, E. Bertheussen, S. B. Scott, X. Liu, A. K. Engstfeld, S. Horch, B. Seger, I. E. L. Stephens, K. Chan, C. Hahn, J. K. Nørskov, T. F. Jaramillo, I. Chorkendorff, *Chem. Rev.* **2019**, *119*, 7610-7672.
- [2] a) L. Ge, H. Rabiee, M. Li, S. Subramanian, Y. Zheng, J. H. Lee, T. Burdyny, H. Wang, *Chem* **2022**, *8*, 663-692; b) H. Shin, K. U. Hansen, F. Jiao, *Nat. Sustain.* **2021**, *4*, 911-919; c) X. Zhang, Y. Wang, M. Gu, M. Wang, Z. Zhang, W. Pan, Z. Jiang, H. Zheng, M. Lucero, H. Wang, G. E. Sterbinsky, Q. Ma, Y.-G. Wang, Z. Feng, J. Li, H. Dai, Y. Liang, *Nat. Energy* **2020**, *5*, 684-692.
- [3] a) C. Chen, Y. Li, P. Yang, *Joule* **2021**, *5*, 737-742; b) M. Ma, E. L. Clark, K. T. Therkildsen, S. Dalsgaard, I. Chorkendorff, B. Seger, *Energy Environ. Sci.* **2020**, *13*, 977-985; c) J. A. Rabinowitz, M. W. Kanan, *Nat. Commun.* **2020**, *11*, 5231.
- [4] J. Gu, S. Liu, W. Ni, W. Ren, S. Haussener, X. Hu, *Nat. Catal.* **2022**, *5*, 268-276.
- [5] a) A. Ozden, F. P. Garcia de Arquer, J. E. Huang, J. Wicks, J. Sisler, R. K. Miao, C. P. O'Brien, G. Lee, X. Wang, A. H. Ip, E. H. Sargent, D. Sinton, *Nat. Sustain.* **2022**, *5*, 563-573; b) Z. Yan, J. L. Hitt, Z. Zeng, M. A. Hickner, T. E. Mallouk, *Nat. Chem.* **2021**, *13*, 33-40; c) C. J. Bondue, M. Graf, A. Goyal, M. T. M. Koper, *J. Am. Chem. Soc.* **2021**, *143*, 279-285.
- [6] a) C. Delacourt, P. L. Ridgway, J. B. Kerr, J. Newman, *J. Electrochem. Soc.* **2008**, *155*, B42; b) J.-B. Vennekoetter, R. Sengpiel, M. Wessling, *Chem. Eng. J.* **2019**, *364*, 89-101; c) M. C. O. Monteiro, F. Dattila, B. Hagedoorn, R. Garcia-Muelas, N. López, M. T. M. Koper, *Nat. Catal.* **2021**, *4*, 654-662.
- [7] a) M. C. O. Monteiro, M. F. Philips, K. J. P. Schouten, M. T. M. Koper, *Nat. Commun.* **2021**, *12*, 4943; b) M. C. O. Monteiro, F. Dattila, N. López, M. T. M. Koper, *J. Am. Chem. Soc.* **2022**, *144*, 1589-1602.
- [8] Y. Xie, P. Ou, X. Wang, Z. Xu, Y. C. Li, Z. Wang, J. E. Huang, J. Wicks, C. McCallum, N. Wang, Y. Wang, T. Chen, B. T. W. Lo, D. Sinton, J. C. Yu, Y. Wang, E. H. Sargent, *Nat. Catal.* **2022**, *5*, 564-570.
- [9] C. P. O'Brien, R. K. Miao, S. Liu, Y. Xu, G. Lee, A. Robb, J. E. Huang, K. Xie, K. Bertens, C. M. Gabardo, J. P. Edwards, C.-T. Dinh, E. H. Sargent, D. Sinton, *ACS Energy Lett.* **2021**, *6*, 2952-2959.
- [10] S. Ren, D. Joulié, D. Salvatore, K. Torbensen, M. Wang, M. Robert, C. P. J. S. Berlinguette, *Nature* **2019**, *365*, 367-369.
- [11] a) L.-C. Weng, A. T. Bell, A. Z. Weber, *Energy Environ. Sci.* **2019**, *12*, 1950-1968; b) D. A. Salvatore, C. M. Gabardo, A. Reyes, C. P. O'Brien, S. Holdcroft, P. Pintauro, B. Bahar, M. Hickner, C. Bae, D. Sinton, E. H. Sargent, C. P. Berlinguette, *Nat. Energy* **2021**, *6*, 339-348.
- [12] H.-G. Qin, F.-Z. Li, Y.-F. Du, L.-F. Yang, H. Wang, Y.-Y. Bai, M. Lin, J. Gu, *ACS Catal.* **2023**, *13*, 916-926.

- [13] a) M. Fan, J. E. Huang, R. K. Miao, Y. Mao, P. Ou, F. Li, X.-Y. Li, Y. Cao, Z. Zhang, J. Zhang, Y. Yan, A. Ozden, W. Ni, Y. Wang, Y. Zhao, Z. Chen, B. Khatir, C. P. O'Brien, Y. Xu, Y. C. Xiao, G. I. N. Waterhouse, K. Golovin, Z. Wang, E. H. Sargent, D. Sinton, *Nat. Catal.* **2023**, *6*, 763-772; b) H.-G. Qin, Y.-F. Du, Y.-Y. Bai, F.-Z. Li, X. Yue, H. Wang, J.-Z. Peng, J. Gu, *Nat. Commun.* **2023**, *14*, 5640.
- [14] M. D. Hossain, Y. Huang, T. H. Yu, W. A. Goddard Iii, Z. Luo, *Nat. Commun.* **2020**, *11*, 2256.
- [15] a) S. Vijay, W. Ju, S. Brückner, S.-C. Tsang, P. Strasser, K. Chan, *Nat. Catal.* **2021**, *4*, 1024-1031; b) Z.-Y. Wu, M. Karamad, X. Yong, Q. Huang, D. A. Cullen, P. Zhu, C. Xia, Q. Xiao, M. Shakouri, F.-Y. Chen, J. Y. Kim, Y. Xia, K. Heck, Y. Hu, M. S. Wong, Q. Li, I. Gates, S. Siahrostami, H. Wang, *Nat. Commun.* **2021**, *12*, 2870; c) T. Zheng, K. Jiang, N. Ta, Y. Hu, J. Zeng, J. Liu, H. Wang, *Joule* **2019**, *3*, 265-278; d) Z.-Y. Wu, P. Zhu, D. A. Cullen, Y. Hu, Q.-Q. Yan, S.-C. Shen, F.-Y. Chen, H. Yu, M. Shakouri, J. D. Arregui-Mena, A. Ziabari, A. R. Paterson, H.-W. Liang, H. Wang, *Nat. Synth.* **2022**, *1*, 658-667.
- [16] Z. Zhang, J. Xiao, X. J. Chen, S. Yu, L. Yu, R. Si, Y. Wang, S. Wang, X. Meng, Y. Wang, Z. Q. Tian, D. Deng, *Angew. Chem. Int. Ed.* **2018**, *57*, 16339-16342.
- [17] Y. Wu, Y. Liang, H. Wang, *Acc. Chem. Res.* **2021**, *54*, 3149-3159.
- [18] a) W. Zhu, R. Michalsky, Ö. Metin, H. Lv, S. Guo, C. J. Wright, X. Sun, A. A. Peterson, S. Sun, *J. Am. Chem. Soc.* **2013**, *135*, 16833-16836; b) A. Goyal, G. Marcandalli, V. A. Mints, M. T. M. Koper, *J. Am. Chem. Soc.* **2020**, *142*, 4154-4161; c) J. Rosen, G. S. Hutchings, Q. Lu, S. Rivera, Y. Zhou, D. G. Vlachos, F. Jiao, *ACS Catal.* **2015**, *5*, 4293-4299; d) N. Zhang, X. Zhang, L. Tao, P. Jiang, C. Ye, R. Lin, Z. Huang, A. Li, D. Pang, H. Yan, Y. Wang, P. Xu, S. An, Q. Zhang, L. Liu, S. Du, X. Han, D. Wang, Y. Li, *Angew. Chem. Int. Ed.* **2021**, *60*, 6170-6176.
- [19] M. T. Greiner, T. E. Jones, S. Beeg, L. Zwiener, M. Scherzer, F. Girgsdies, S. Piccinin, M. Armbrüster, A. Knop-Gericke, R. Schlögl, *Nat. Chem.* **2018**, *10*, 1008-1015.
- [20] a) J. K. Nørskov, F. Abild-Pedersen, F. Studt, T. Bligaard, *Proc. Nat. Acad. Sci.* **2011**, *108*, 937-943; b) J. K. Nørskov, F. Studt, F. Abild-Pedersen, T. Bligaard, *Fundamental concepts in heterogeneous catalysis*, John Wiley & Sons, **2014**.
- [21] a) X. Ren, J. Zhao, X. Li, J. Shao, B. Pan, A. Salamé, E. Boutin, T. Groizard, S. Wang, J. Ding, X. Zhang, W.-Y. Huang, W.-J. Zeng, C. Liu, Y. Li, S.-F. Hung, Y. Huang, M. Robert, B. Liu, *Nat. Commun.* **2023**, *14*, 3401; b) H. Li, Y. Pan, Z. Wang, Y. Yu, J. Xiong, H. Du, J. Lai, L. Wang, S. Feng, *Nano Res.* **2022**, *15*, 3056-3064.
- [22] X. Zhang, Z. Wu, X. Zhang, L. Li, Y. Li, H. Xu, X. Li, X. Yu, Z. Zhang, Y. Liang, H. Wang, *Nat. Commun.* **2017**, *8*, 14675.
- [23] X. Wu, J. W. Sun, P. F. Liu, J. Y. Zhao, Y. Liu, L. Guo, S. Dai, H. G. Yang, H. Zhao, *Adv. Funct. Mater.* **2022**, *32*, 2107301.
- [24] a) H. Rabiee, L. Ge, X. Zhang, S. Hu, M. Li, Z. Yuan, *Energy Environ. Sci.* **2021**, *14*, 1959-2008; b) D. M. Weekes, D. A. Salvatore, A. Reyes, A. Huang, C. P. Berlinguette, *Acc. Chem. Res.* **2018**, *51*, 910-918.
- [25] a) C.-T. Dinh, F. P. García de Arquer, D. Sinton, E. H. Sargent, *ACS Energy Lett.* **2018**, *3*, 2835-2840; b) M. Sassenburg, R. de Rooij, N. T. Nesbitt, R. Kas, S. Chandrashekar, N. J. Firet, K. Yang, K. Liu, M. A. Blommaert, M. Kolen, D. Ripepi, W. A. Smith, T. Burdyny, *ACS Appl. Energy Mater.* **2022**, *5*, 5983-5994.
- [26] Y. Wu, Z. Jiang, X. Lu, Y. Liang, H. Wang, *Nature* **2019**, *575*, 639-642.
- [27] J. E. Huang, F. Li, A. Ozden, A. Sedighian Rasouli, F. P. García de Arquer, S. Liu, S. Zhang, M. Luo, X. Wang, Y. Lum, Y. Xu, K. Bertens, R. K. Miao, C.-T. Dinh, D. Sinton, E. H. Sargent, *Science* **2021**, *372*, 1074.
- [28] a) X. Lu, C. Zhu, Z. Wu, J. Xuan, J. S. Francisco, H. Wang, *J. Am. Chem. Soc.* **2020**, *142*, 15438-15444; b) Z. Zhang, L. Melo, R. P. Jansonius, F. Habibzadeh, E. R. Grant, C. P. Berlinguette, *ACS Energy Lett.* **2020**, *5*, 3101-3107.
- [29] O. Pedersen, T. Colmer, K. Sand-Jensen, *Front. Plant Sci.* **2013**, *4*.
- [30] W. Deng, P. Zhang, B. Seger, J. Gong, *Nat. Commun.* **2022**, *13*, 803.

Table of contents



Without the assistance of metal cations, CoPc@CNT itself stabilizes *CO₂ intermediates at the acidic interface, and thus enables CO₂ conversion in pure acid, even at pH = 1. As for Au/Ag, CO₂ adsorption step is completely suppressed by the high coverage of H, causing only hydrogen evolution reaction to occur.